UPCommons

Portal del coneixement obert de la UPC

http://upcommons.upc.edu/e-prints

A Unified Power Flow Controller Using a Power Electronics Integrated Transformer

M. A. Elsaharty, *Member, IEEE*, A. Luna, *Member, IEEE*, J. I. Candela, *Member, IEEE* and
Pedro Rodriguez, *Fellow, IEEE*

Abstract-- **This paper presents a Unified Power Flow Controller (UPFC) application of the Custom Power Active Transformer (CPAT); a power electronics integrated transformer which provides services to the grid through its auxiliary windings. The CPAT structure integrates three single-phase transformers into one shunt-series combining transformer. This integration empowers a sub-station with the capability of dynamically regulating the terminal voltage and current of a transformer through isolated power electronics converters. This paper investigates the CPAT's capability to provide UPFC services which includes power flow control, reactive power compensation, voltage regulation and harmonics elimination. Simulations of the CPAT-UPFC with a stiff grid and a 5-bus power system demonstrates its functionality as an inter-bus coupling transformer that provides the required grid services. Moreover, the impact of the CPAT-UPFC during load perturbations on the power system is investigated to further validate its transient and steady-state response. Furthermore, an experimental prototype reveals the operation of the three-phase CPAT-UPFC confirming its stable operation according to the theoretical expectations.**

Index Terms-- **Power transformers, Magnetic circuits, Power control, Power transmission.**

I. INTRODUCTION

THE increased demand for distributed generation to facilitate momentous contributions to the grid has faced several challenges and technical issues. Owing to the intermittent behavior of renewable generation and the ever-growing need of electrical energy, the construction and operation of substations has undergone several developments to address these challenges [1]. To guarantee a reliable, sustainable and intelligent electric network, integration of monitoring and control functionalities throughout the power system have evolved to respond to such demands [2]. Such functionalities have been commissioned through power electronics converters that has proven several beneficial impacts on the distribution network [3-5] and transmission network [6-8].

Flexible AC Transmission Systems (FACTS) have proven their capability in providing services to effectively support the transmission and distribution systems, increasing their reliability, quality and stability [9]. Among such devices, the UPFC is considered the most versatile device to reduce line congestion and increase existing lines capacity. Connection of power electronics converters to provide UPFC services have either been achieved through bulky isolation transformers, complex multilevel topologies or back-to-back converters handling the rated line power [10-12]. Transformer-less approaches involving multilevel topologies arises from the need of eliminating requirement of bulky isolation transformers. However, such topologies handle the full rated line voltage which typically requires a complex configuration.

The use of transformers to connect shunt and series power electronic devices to the power system is an effective solution due to the isolation they provide. However, size, cost and footprint are another concern when considering high power compensation systems. To address such concerns, the integration of power electronic devices in a typical transformer has been observed in recent literature aiming for the use of off-the-shelf converters [13-15] or construction of a power electronics-based transformer [16]. However, these approaches have either addressed one type of compensation [13], specific applications [14-15] or require high power and complex architectures [16].

The CPAT presented in [17] and [18] shows a monolithic transformer core structure that integrates series and shunt power electronics converters to a distribution transformer. A CPAT is comparable to a Sen Transformer [15] in the case of combining multiple transformers into a single unit. However, the CPAT carries several advantages over a Sen Transformer which is mainly due to the presence of power electronics converters in a CPAT as opposed to the step response of a Sen Transformer. The CPAT has been presented to provide shunt services such as reactive power compensation, harmonics elimination and inrush current mitigation. Several of these services cannot be provided by a Sen Transformer. However, the CPAT has been investigated for single-phase applications and solely for distribution network as a Unified Power Quality Conditioner (UPQC). Based on the theory of operation of a CPAT, transmission applications can also be realized since the provided auxiliary windings can be used for any shunt-series application.

Several approaches have been presented in literature that resolves isolation requirement through transformer-less approaches [19-20] or power-electronics based transformers

[10]. Even though such configurations have been practically utilized in several applications [21-22] which eliminates the requirement of bulky line transformers for isolation, the complexity of the power electronics configuration creates a challenge [23]. Since bulky power transformers present an essential element in a power system to match voltage levels between different busses, the CPAT integrates both series and shunt transformers within such power transformers. In this case, an isolated UPFC using fractional power converters can be installed by replacing any power transformer with a CPAT. Thus, this provides an integrated UPFC within any power transformer.

This paper proposes the CPAT-UPFC using three single-phase CPATs to regulate power flow between the primary and secondary windings, as well as provide reactive power compensation and harmonics elimination. The three-phase configuration of a CPAT is presented, modeled and analyzed for power flow control applications based on its equivalent magnetic circuit. The CPAT-UPFC has been tested through simulations and experiments for power flow control between two stiff grids. Moreover, the CPAT-UPFC has been simulated as a substation transformer in a 5-bus power system for power flow control and operating under load perturbations in the power system. Finally, the acquired real-time simulations and experimental results reveal the capability of a CPAT-UPFC to provide such services effectively.

This paper is organized as follows : in Section II, the theory of operation of a three-phase CPAT and its equivalent models are presented. Section III proposes the control of a three-phase CPAT for a UPFC application. Section IV presents simulation evaluation of the CPAT-UPFC under stiff grid connection. Section V evaluates the CPAT-UPFC on an experimental platform and as a substation transformer in a 5-bus power system in a real-time simulation. Finally, conclusions are summarized in Section VI.

II. THEORY OF OPERATION

A. Configuration

The core construction of a single-phase CPAT that combines series and shunt windings in a transformer has been presented in [17-18]. The operation principle of the CPAT is based upon the theory that windings wound over common limbs are equivalent to shunt electric circuits and that windings wound over parallel limbs are equivalent to series electric circuits. Taking these principles into account, the configuration in Fig.1 represents a three-phase CPAT in a transmission application. The configuration consists of three single-phase CPATs equipped with a three-phase back-to-back converter. Each CPAT is labelled $CPAT_p$, where p represents the phase number. Winding voltages and currents of each CPAT are represented by v_{pk} and i_{pk} where k represents the winding number. The primary and secondary windings of a CPAT (k=1, k=4) are connected to the grid as in a typical transformer. A three-phase back-to-back converter is connected to the shunt and series windings (k=2, k=3) to control the shunt winding current and series winding voltage. The shunt converter provides services to the primary winding such as harmonic elimination and reactive power compensation; it also regulates the DC bus voltage. The series

converter controls active and reactive power through the secondary winding to operate as a UPFC.
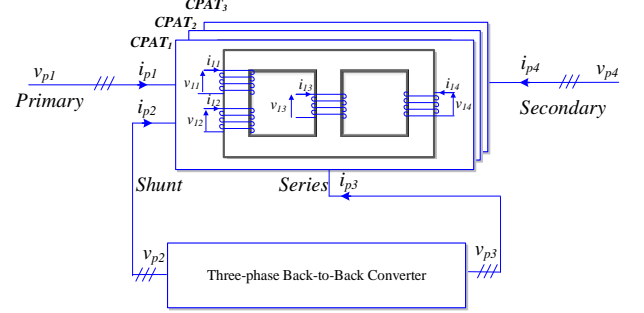

Fig. 1. Three-phase CPAT configuration using three single-phase CPATs and a back-to-back converter.

B. Modeling

1. NON-LINEAR TRANSFORMER MODEL

By discretizing the magnetic flux paths in the core (Fig. 2), an equivalent model (Fig. 2 (a)) can be deduced. Fig. 2(a) shows m number of limbs and k winding types, with k=1 (primary), 2 (shunt), 3 (series), and 4 (secondary). Fluxes present in this circuit are characterized as core linkage fluxes (Φ_{cm}), winding fluxes (Φ_k), leakage fluxes per winding (Φ_{Lk}), and core leakage flux (Φ_0). Core limbs and yokes are represented by non-linear reluctances $\Re_Y$ and $\Re_L$, with a value calculated based on the B-H characteristics of the core material. A non-linear reluctance is modelled as a controlled magneto-motive source in a closed-loop between input flux and output magneto-motive force (F), as shown in Fig. 2(b). This model would produce an opposing magneto-motive force based on the limb or yoke length (l), area (A) and the core B-H characteristics shown in Fig. 3.

Winding leakage reluctances ($\Re_k$) and core leakage reluctance ($\Re_0$) are represented by linear reluctances. Leakage reluctances are evaluated using the flux path length, mean area and relative permeability of air (μ_0=4π10^{-7}). The flux generated by each winding is linked to a winding electric circuit, shown in Fig.2(c), to model winding losses and core equivalent losses. For any applied winding voltage (v_k), the equivalent transformer winding current (i_k) is dependent on winding resistance (R_k), equivalent core loss resistance (R_c) and effective winding current (i_{ek}). The effective current is calculated based on the effective magneto-motive force (F_k) of the winding and number of turns (N_k), as shown in Fig.2(c). The winding flux in the magnetic circuit is deduced from the effective voltage (v_{ek}) in the winding electric circuit.
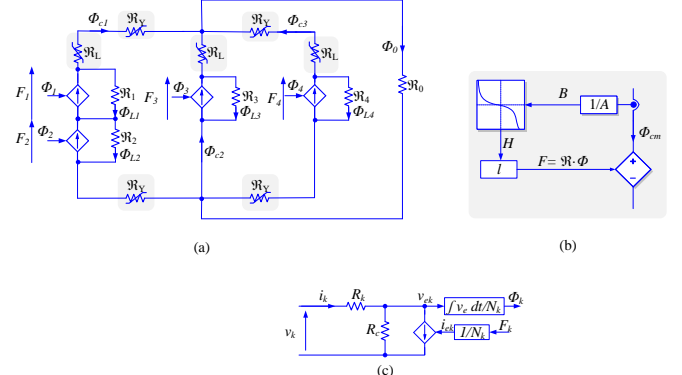

Fig. 2. Equivalent magnetic circuit model of a single-phase CPAT. (a) core equivalent magnetic circuit, (b) non-linear core reluctance model, and (c) winding equivalent electric circuit.

2. Linear Transformer model

A linear representation of the model can be derived through duality transformation of the magnetic circuit (Fig. 2) to its equivalent electric circuit shown in Fig. 3. Non-linear core impedances are assumed to be constant and large enough to sustain perfect couplings between primary, shunt, series and secondary windings. Core magnetizing impedances and core loss resistances are represented by L_{e1}, L_{e2} and L_{e3} and R_{e1}, R_{e2} and R_{e3} respectively. Transformer leakage inductances and zero-sequence magnetizing inductance are represented by L_k and L_0 respectively. The equivalent circuit (Fig. 3) is identical to the circuit of a three-phase transformer, apart from two windings on the centre and secondary limbs. The parameters of this circuit can be determined based on the typical transformer tests methodology [24] for low- and mid-frequency transient simulations.
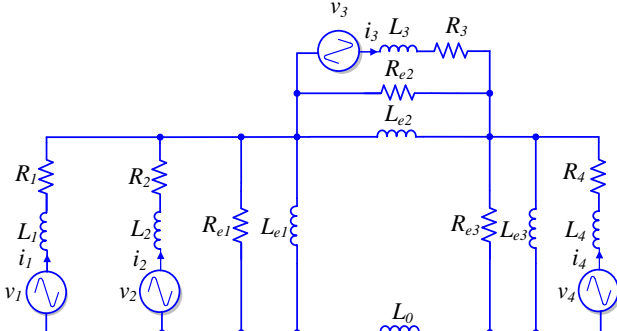

Fig. 3. Equivalent linear electric circuit of a single-phase CPAT.

3. Power Converters model

The configuration in Fig.1 was implemented using the topology illustrated in Fig.4. A three-phase back-to-back converter was connected to the shunt and series windings of the CPAT. As in a typical UPFC, the shunt converter operated as a current controlled voltage source inverter (CCVSI) equipped with an LCL filter, to attenuate switching frequency harmonics. The filter parameters L_{1sh}, C_{sh} and L_{2sh} were selected based on the required attenuation of switching frequency harmonics and resonance frequency. Damping of filter resonance was achieved through the shunt damping resistance (R_{sh}). The converter was connected in a three-phase 4-wire topology to facilitate the capacity to inject triplen harmonic current in the shunt windings. The magnetizing

harmonic currents required by the transformer were evident. Therefore, injection of such harmonic current components through the shunt winding would eliminate their requirement from the grid. The shunt converter controller maintains a constant DC bus voltage (v_{dc1}, v_{dc2}) over each DC bus capacitor (C_{dc}) and controls the shunt converter current (i_{p2sh}). Primary voltage (v_{p1}) and current (i_{p1}) were measured to synchronize the shunt converter voltage (v_{p2}) with the v_{p1} and to provide the required services to i_{p1}. The output PWM signals of the shunt converter controller drove the converter switches of the shunt converter to control the shunt current according to the required reference.

The series inverter operated as a voltage source inverter, equipped with an LC filter to attenuate switching frequency harmonics of the output voltage (v_{p3}). Similarly, the filter parameters L_{ser}, C_{ser} and R_{ser} were selected based on the required attenuation of switching frequency harmonics and resonance damping. The secondary voltage (v_{p4}) and current (i_{p4}) were measured to control the series voltage (v_{p3}) according to the required services provided to i_{p4}. The output PWM signals from the series converter controller drove the series inverter to achieve the required reference series voltage. As shown in Fig.4, each phase of the primary, shunt, series and secondary winding were linked in a common CPAT core, resulting in a three-phase CPAT configuration.

An average model of both converters, accompanied by the linear model of the CPAT, are shown in Fig. 5. This system can be utilized to investigate the performance of a CPAT in low- to mid-frequency transients. The average model neglects the effect of switching frequency harmonics by using a linearly controlled voltage source, as shown in Fig. 5. Because harmonics are not considered in this model, a three-phase three-wire converter configuration was used. The common DC bus was emulated at each model sample instant (v_{dc}) using the measured shunt converter power (P_2) and series converter power (P_3) as demonstrated in (2).

$$v_{dc1} = v_{dc2} = -\frac{1}{2}\int \frac{P_2 + P_3}{C_{dc}v_{dc}}dt \qquad (1)$$
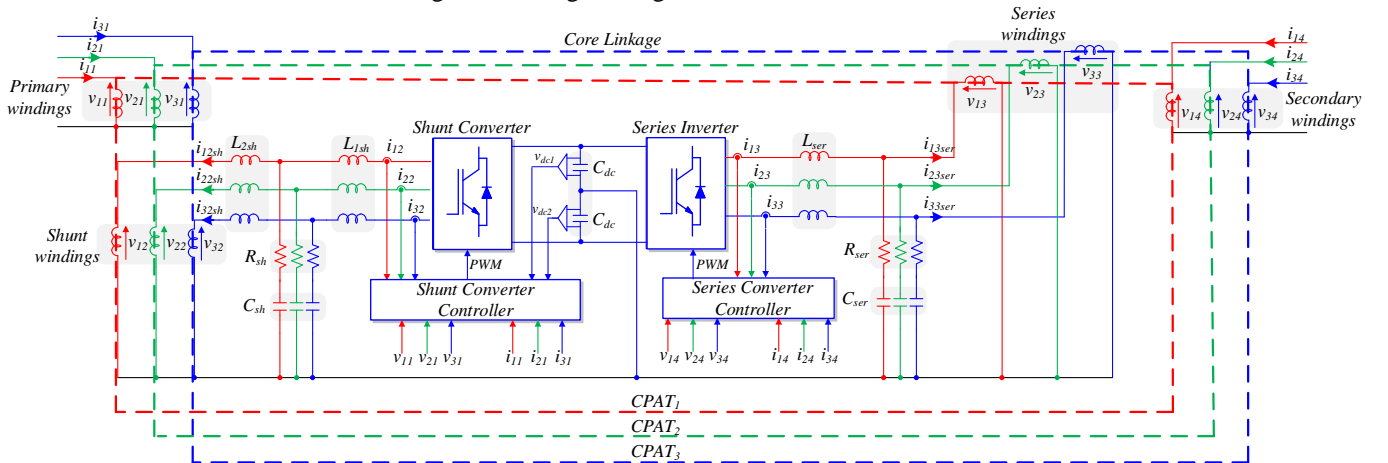

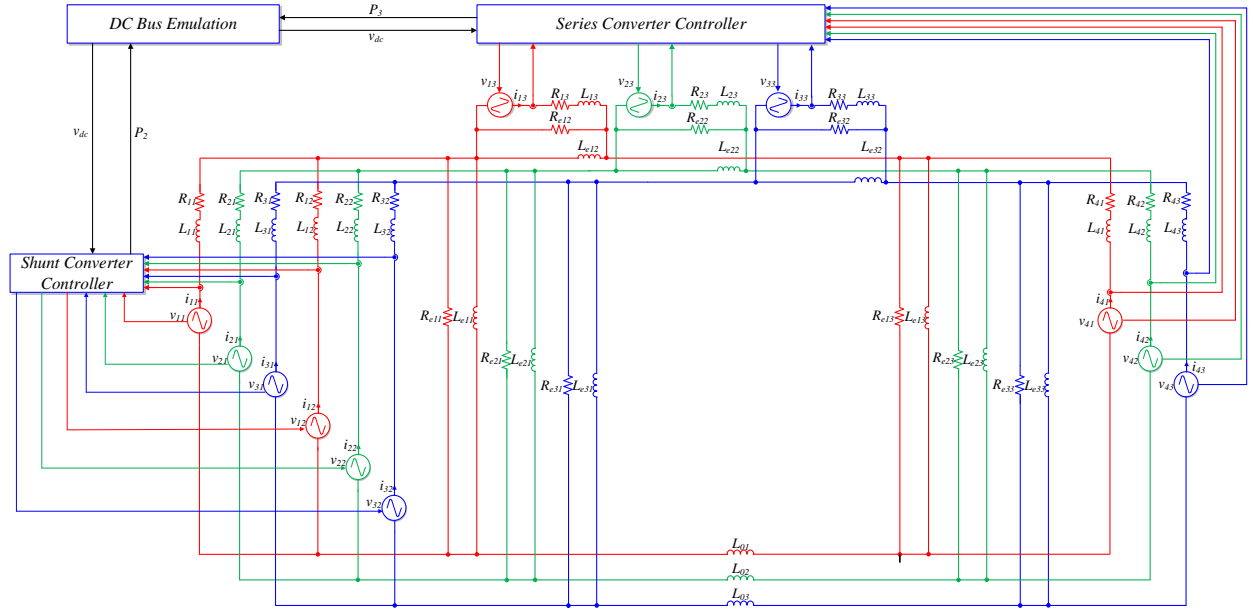Fig. 4. Back-to-back converter topology for the three-phase CPAT.

Fig. 5. Average model of the three-phase CPAT and back-to-back converter.

III. CONTROL OF THREE-PHASE CPAT-UPFC

The control architecture of the CPAT-UPFC is illustrated in Fig.6 and Fig. 7 consisting of two independent controllers. As discussed earlier, the objectives of the shunt converter controller shown in Fig.6 are as follows: to maintain a constant DC bus voltage based on the reference DC bus voltage (V_{dc}^*), to regulate reactive power through the primary based on the reference reactive power (Q_1^*), and to eliminate harmonic components present in the primary current. The measured values for these objectives are primary grid voltage (v_{p1}), primary grid current (i_{p1}), shunt converter current (i_{p2}) and DC bus voltages (v_{dc1} and v_{dc2}). The series converter controller shown in Fig. 7 simultaneously controls the active and reactive power flow through the secondary winding of the CPAT, based on the reference active (P_4^*) and reactive (Q_4^*) power. Moreover, Q_4^* can be set through a controller that regulates a load bus voltage (V_{load}). The measured variables for these control objectives are secondary grid voltage (v_{p4}), secondary grid current (i_{p4}) and load bus voltage (v_{load}). Both i_{p2} and series converter current (i_{p3}) are also used for over-current protection in each converter.

Measurements from each architecture were sampled through the Sample and Hold to obtain the n sample value of each measured variable. The synchronization system uses the measured voltages to determine their equivalent frequency (ω), synchronizing signals ($sin(\omega t)$, $cos(\omega t)$), magnitude (V) and synchronous reference-frame components (v_α, v_β). These signals, along with the measured variables and reference variables, were passed to the equivalent controller, which determined the required modulation of the converter (M). Finally, the PWM module determined the equivalent switching state of each switch (g) to achieve the required control objectives.

The shunt controller shown in Fig.6 has been previously discussed in [17] and [18] which achieves the required control objectives. A Proportional Resonant (PR) controller regulates the shunt converter current according to the required reference shunt current (i_{p2}^*). The reference consists of a fundamental component (i_{p2f}^*) which is used to regulate the DC bus voltage and reactive power through the primary as well as a harmonics component (i_{p2h}^*) which is used to regulate the harmonic currents present in i_{p1}. Harmonic components injected through the shunt converter are determined through a Resonant Controller tuned to the required attenuation frequencies of the primary current (i_{p1}). The DC bus voltage is regulated through two Proportional Integral (PI) controllers that regulate the average DC bus voltage (v_{dc}) and the balance between both upper and lower DC voltages (v_{dc1} and v_{dc2}). Reactive power through the primary is regulated through a PI controller that determines the required reactive current to be injected through the shunt converter to obtain the required reference Q_1^*. The feedback reactive power (Q_1) is calculated using (2).

$$Q_1 = \frac{1}{\sqrt{3}}\begin{bmatrix} v_{11} & v_{21} & v_{31} \end{bmatrix}\begin{bmatrix} 0 & -1 & 1 \\ 1 & 0 & -1 \\ -1 & 1 & 0 \end{bmatrix}\begin{bmatrix} i_{11} \\ i_{21} \\ i_{31} \end{bmatrix} \quad (2)$$

The series controller shown in Fig.7 consists of three stages: reference reactive power calculation, secondary current calculation and secondary current controller. The reference reactive power (Q_4^*) is set either manually or through a secondary voltage controller that determines the required reactive power to maintain the reference load voltage (V_{load}^*). The secondary current calculation determines the equivalent stationary reference-frame secondary current ($i_{\alpha4}$, $i_{\beta4}$), based on the reference active and reactive power (P_4^*, Q_4^*) using the stationary reference-frame secondary voltage ($v_{\alpha4}$, $v_{\beta4}$). Equation (3) summarises the calculations [25].

Using the secondary synchronizing signals ($sin(\omega t)_4$, $cos(\omega t)_4$), the $i_{\alpha4}$ and $i_{\beta4}$ are transformed to their equivalent three-phase quantities (i_{p4}^*). A PR controller tuned to the fundamental frequency (ω_4) controls the secondary current (i_{p4}) to match the reference i_{p4}^*. The resultant reference series voltage (v_{p3}^*) is divided by the DC bus voltage (v_{dc}) to determine the modulation index of the series converter (M_{p3}).

$$\begin{bmatrix} i_{\alpha4} & i_{\beta4} \end{bmatrix} = \frac{1}{v_{\alpha4}^2 + v_{\beta4}^2}\begin{bmatrix} P_4^* & Q_4^* \end{bmatrix}\begin{bmatrix} v_{\alpha4} & -v_{\beta4} \\ v_{\beta4} & v_{\alpha4} \end{bmatrix} \quad (3)$$
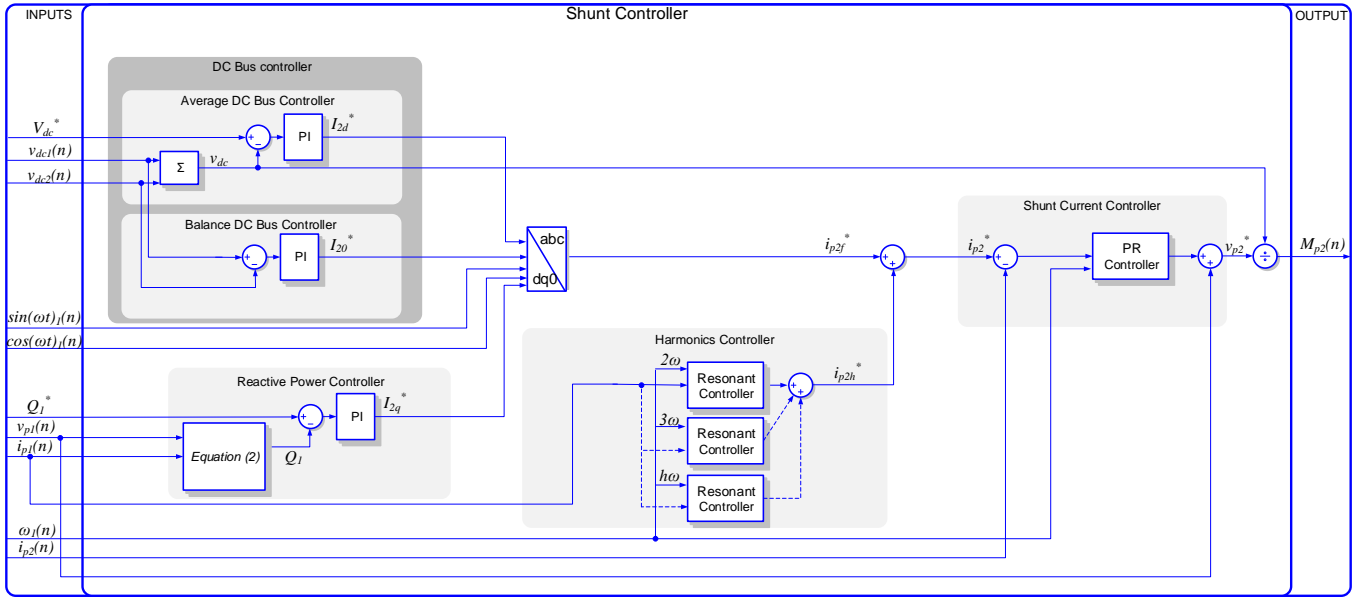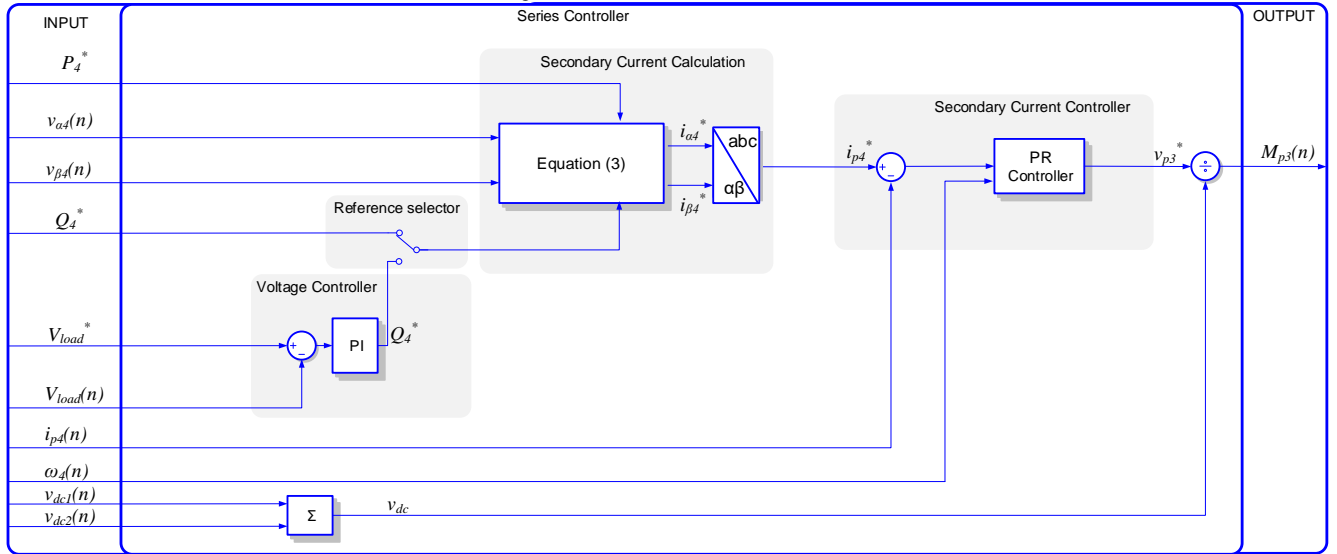
Fig. 6. Shunt Controller block structure.

Fig. 7. Series Controller block structure.

IV. SIMULATION RESULTS

Using the modelling approach discussed in the previous Section II, the CPAT configuration in Fig. 4 was modelled based on the parameters presented in Table I. The transformer model consists of number of turns N, limb length l_L, yoke length l_Y and limb area A.

The primary and secondary winding were connected to a common stiff grid as shown in Fig.8. In this condition, there is no power flow between the primary and secondary since both are excited by an equal voltage. Therefore, only magnetizing current of the CPAT would be divided between both windings to excite the core. Meanwhile, with both shunt and series controllers disabled, the shunt and series converters injected zero current and voltage respectively.

The primary current consisted mainly of 3rd, 5th and 7th-order harmonics, as shown in Fig.9. Because there was no power flow between the primary and secondary in this scenario, the primary current consisted mainly of fundamental

CPAT magnetizing current and DC bus regulation current. The shunt harmonics controller tuned to these frequencies eliminated these components from the primary current waveform, as shown in Fig.10. Uncompensated higher-order harmonics were not a concern because these harmonic currents would not be magnified, as the primary current increased beyond the magnetizing current and yet would remain below standards. The shunt reactive power controller, set with a reference of 0 VAR, was enabled so that the shunt converter supplied the reactive power required by the CPAT, as shown in Fig.11.

The secondary current controller was enabled, with a reference of 5 kW and 0 kVAR power flow between the primary and secondary (Fig. 12). The series converter supplied reactive power to the series winding to alter the equivalent impedance between the primary and secondary windings. The primary power changed at that instant too because the secondary injected power to the grid, which was received by the primary (Fig.13). The DC bus controller maintained a

constant DC bus voltage throughout the operation, as illustrated in Fig.14. The resultant primary and secondary current waveform from this reference is shown in Fig.15. The diagram illustrates the effectiveness of the harmonics controller in attenuating the primary current harmonics at the tuned frequencies throughout the operation

TABLE I
Parameters of the Non-linear CPAT and Converter Model

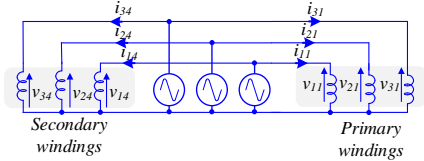| Parameter	Value
Grid voltage/phase	220V
$v_{p1}, v_{p2}, v_{p3}, v_{p4}$	240V, 240V, 480V,240V
$i_{p1}, i_{p2}, i_{p3}, i_{p4}$	70A, 7.2A, 7.2A, 70A
R_{pk}, R_{pm}	0.002 p.u., 500 p.u.
l_L, l_Y, A	0.51m, 0.3m, 0.0156 m^2
$N_{p1}, N_{p2}, N_{p3}, N_{p4}$	50, 50, 100, 50
V_{dc}	700V
Sampling Frequency, Switching Frequency	10kHz
C_{dc}	20mF
$L_{1sh}, L_{2sh}, L_{ser}$	6mH, 2mH, 7mH
R_{sh}, R_{ser}	4.7Ω, 2.35 Ω
C_{sh}, C_{ser}	5µF, 10µF

Fig. 8. Stiff grid connection to primary and secondary windings.
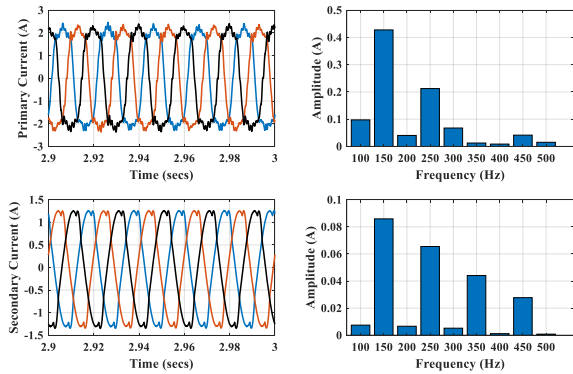

Fig.9. Primary and secondary current waveform with harmonics spectrum analysis of both currents while shunt converter disabled.
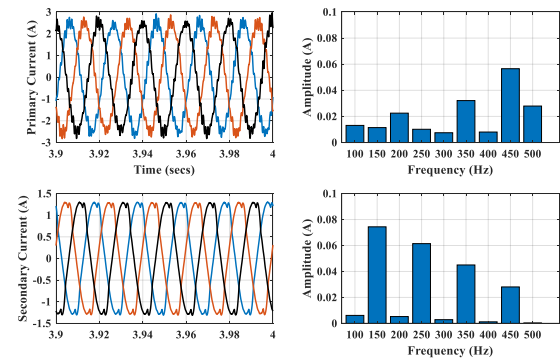

Fig. 10. Primary and secondary current waveform with harmonics spectrum analysis of both currents while shunt converter enabled.
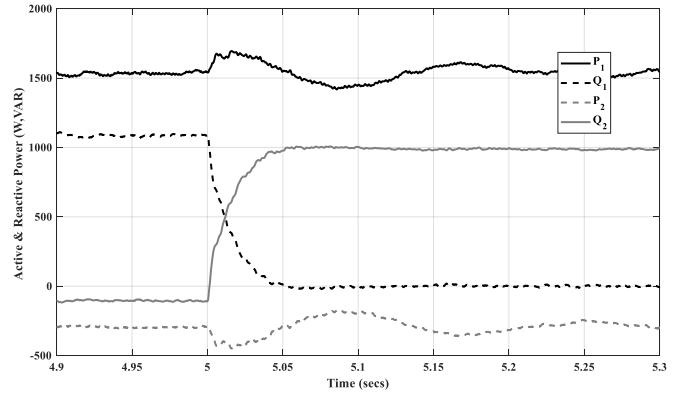

Fig. 11. Active and reactive power through the primary and shunt winding with enabled Reactive Power Controller.
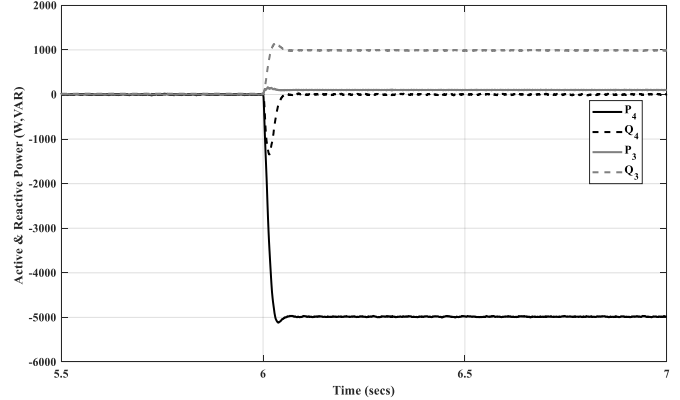

Fig. 12. Active and reactive power through the secondary and series winding during activation of the Secondary Current Controller.
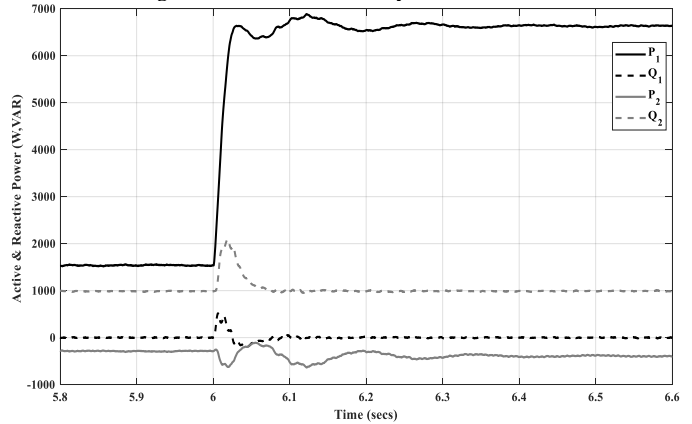

Fig. 13. Active and reactive power through the primary and shunt windings during step change in reference output power.
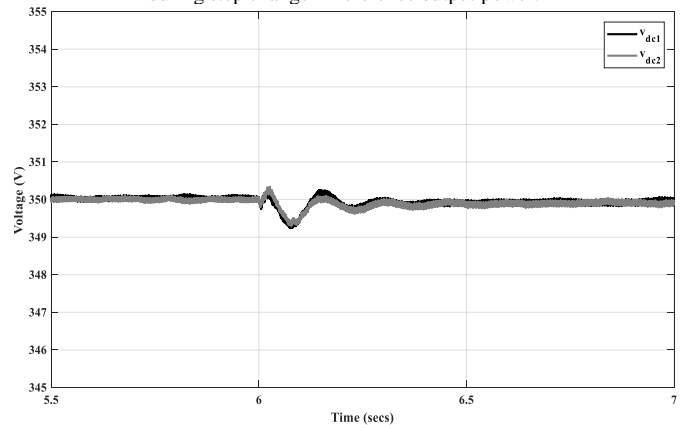

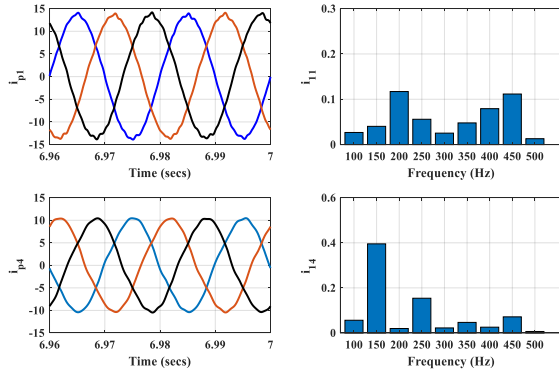Fig. 14. DC bus voltage during change in reference output power.

Fig. 15. Primary and secondary current waveform and harmonics spectrum with all controllers enabled.

V. EXPERIMENTAL RESULTS

The laboratory set-up shown in Fig. 16 consisted of three multi-winding three-phase transformers and two 5-kW back-to-back converters, connected according to the configuration in Fig. 4. All transformer parameters are presented in Table I. The primary and secondary windings were connected according to the configuration shown in Fig.8. Each converter was controlled through a DS1103 controller board, with a sampling and switching frequency of 10kHz.

To investigate the operation of a three-phase CPAT in a power system, the CPAT was used in a 5-bus power system real-time simulation case study shown in Fig. 17 using OPAL-RT. The case study set-up consisted of two machines, G1 and G2, rated 1000MVA and 1200MVA, respectively. The CPAT was placed between the generator bus (B1) and the transmission bus (B3) to replace a 1000MVA step-up transformer for the 50km transmission line to the load bus (B5). The CPAT was modelled according to the configuration shown in Fig. 5 with the equivalent parameters presented in Table II.

In this system, the series winding of the CPAT-UPFC was utilized to control active power through the 50km transmission line and regulate the load bus voltage (V_{load}). Because the CPAT-UPFC was not connected at the load bus, a 100msec delay in the measured load bus voltage was considered to account for communication delay [26]. The CPAT also regulated reactive power absorbed between B1 and B3 through its shunt winding. A 500MW,750MVAR load was suddenly connected on bus B5 to investigate the effectiveness of a CPAT to regulate load bus voltage and power flow through the system.
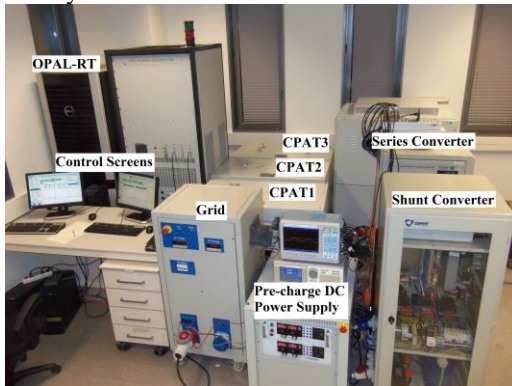

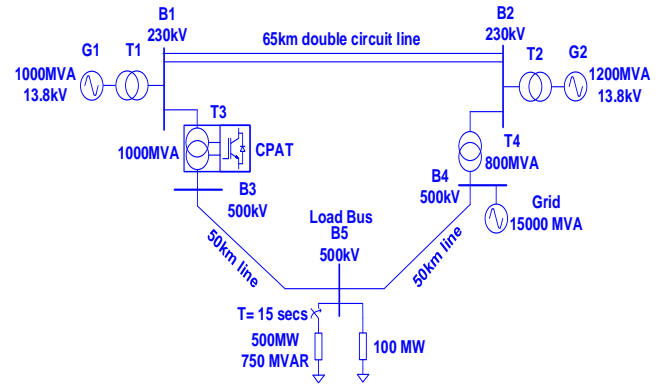Fig. 16. Laboratory setup layout of the three-phase CPAT-UPFC.

Fig. 17. Single-line diagram of 5-bus power system case study with a three-phase CPAT model.

TABLE II
Parameters of the Average CPAT and Converter Model

Parameter	Value
Rated Power/CPAT	333MVA
v_{p1}, v_{p2}, v_{p3}, v_{p4}	138.5kV, 138.5kV, 138.5kV,288.6kV
R_{pk}, R_{epm}	0.002 p.u., 500 p.u.
L_{pk}, L_{epm}, L_0	0.002 p.u., 500 p.u., 0.003 p.u.
v_{dc1}, v_{dc2}	250kV
Control sampling frequency	10kHz

A. Stiff grid

The set-up was initiated with the DC bus controller enabled, to maintain a constant DC bus for the set-up operation. During this state, the harmonic spectrum of the primary current consisted mainly of 3rd and 5th-order harmonics, of 55% and 18% magnitude respectively, as shown in Fig. 18(a). The 2nd and 7th-order harmonics represented 2% of the magnetizing current. With the harmonics controller tuned to 3rd, 5th and 7th-order frequencies, the harmonics present in the primary current were mitigated, with each component reduced by more than 95% (Fig. 18 (b)).

The reactive power compensation controller was set to decrease the reactive power through the primary to zero, as shown in Fig. 19. At that instant, the shunt winding current increased, so that the 1.8 kVAR required from the primary was supplied through the shunt converter. The 1.8 kVAR represented the CPAT magnetizing power. At steady-state, the shunt converter supplied the reactive power required by the CPAT and secondary winding.

The series converter was set with a -5kW reference for secondary power, so that an extra 5 kW would be absorbed from the primary to the secondary and fed to the grid. Activation of the secondary current controller with the pre-set reference resulted in an increase in the secondary current as shown in Fig. 20 which corresponds to the required output power. The series converter supplied mainly reactive power, using approximately 25% of the rated converter power, to change the power flow in the transformer by 10% of its rated power. At the same instant, the primary current increased to supply the required active power by the secondary winding and transformer core (Fig. 21). Moreover, the shunt converter absorbed an extra 570 W to maintain a constant DC bus voltage while supplying the series converter with its required active power.

B. 5-bus Power System

Using the OPAL-RT, a real-time simulation of the 5-bus power system was performed to investigate the stability of the power system with the CPAT in operation. This analysis examined the operation of the CPAT-UPFC system, with and without compensation, under a sudden load connection in the power system (Fig. 17). All power references were set to the nominal power-flow values before load connection with P_4^*=330MW, Q_4^*=-30MVAR, Q_1^*=-25MVAR, V_{load}=500kV and v_{dc}^*=500kV. Once these references were set, the behaviour of the system was compared to a system without a CPAT-UPFC controller (i.e. both shunt and series converters disabled). Fig.22 illustrates the effect of load connection on the power-system sources. The CPAT displayed significant damping on G1 (Fig.22(a)), shifting the oscillations to G2 and to the grid. Moreover, reactive power requirements by G1 were reduced, as shown in Fig.22(a) because the CPAT mainly supplied reactive power (Fig.22(b)) to compensate for the load voltage drop.

The reactive power flowing through the transformer primary winding, shown in Fig.22(b) was significantly reduced because the shunt converter (Q_2 in Fig.22(b)) supplied such power. In addition, the shunt converter supplied the increased reactive power demand at the load bus. Primary and secondary active power damping, shown in Fig.22(b) were achieved through the series converter controller. The damping effect was evident in the series converter action (P_3 in Fig.22(b)) as it initially absorbed active power to maintain a constant secondary current at the load connection instant. Later, the series converter supplied the steady-state required active and reactive power to maintain the required secondary power reference.

The regulation effect on the load bus voltage and DC bus voltage during load connection is shown in Fig.23. The communication delay affected the damping of the load voltage oscillation. However, the voltage drop of 5% at the load bus was compensated for through the CPAT. The tuning effect of the voltage controller on the response with a communication delay was not investigated in this study.

The DC bus voltage increased during the load connection, as shown in Fig.23, because the series converter initially absorbed active power (P_3 in Fig.22(b)). Fig.23 shows the DC bus recharging to maintain a constant voltage when the shunt converter absorbed active power and injected reactive power to the grid, as presented in Fig.22(b).
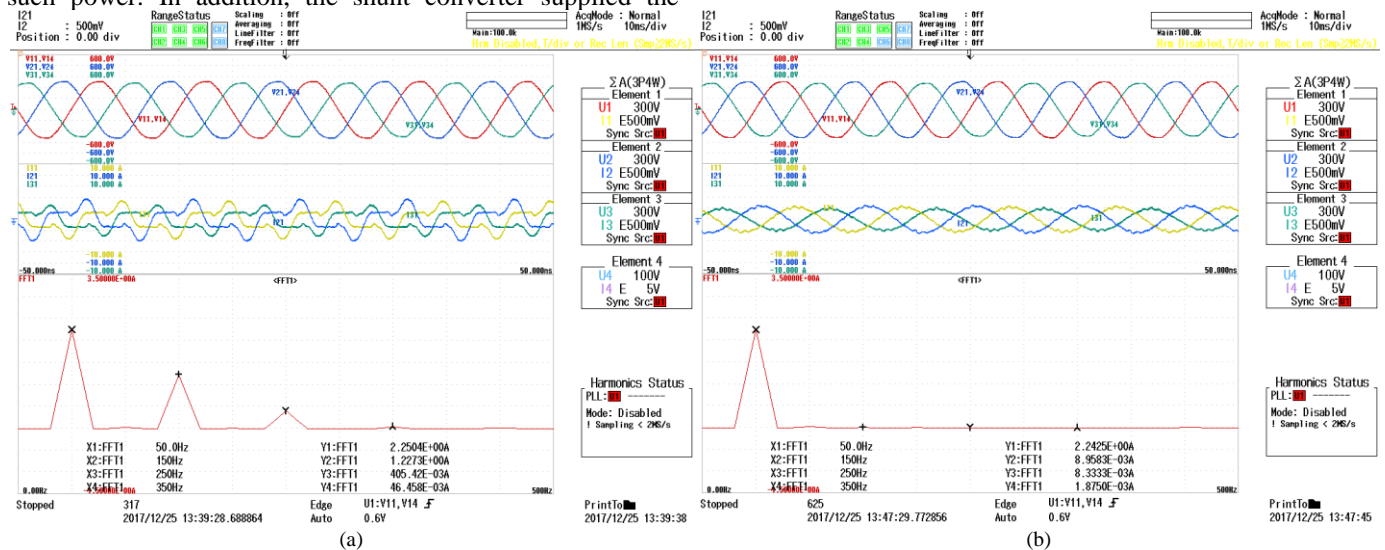

(a)   (b)

Fig. 18. Experimental primary current waveform and harmonics spectrum. (a) without harmonics compensation and (b) with harmonics compensation.
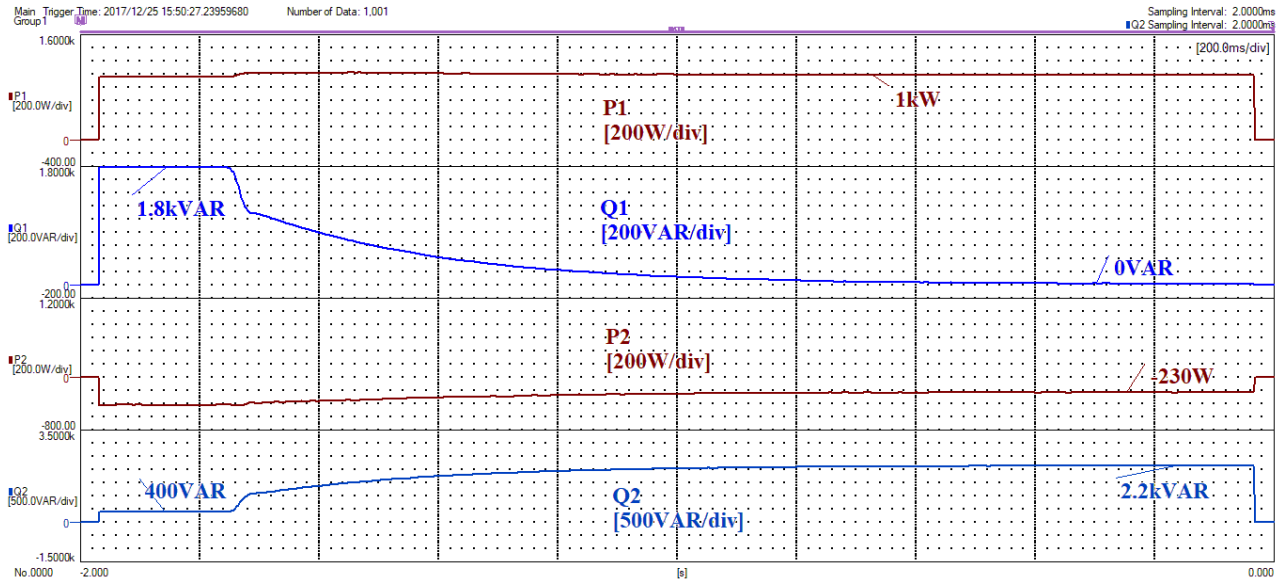
P1
[200W/div]

1kW

Q1
[200VAR/div]

1.8kVAR

0VAR

P2
[200W/div]

-230W

Q2
[500VAR/div]

400VAR

2.2kVAR

Fig. 19. Experimental results of shunt converter operation with Reactive Power Compensator controller set to 0kVAR (200ms/div).

P4
[1kW/div]

-5kW

Q4
[200VAR/div]

P3
[100W/div]

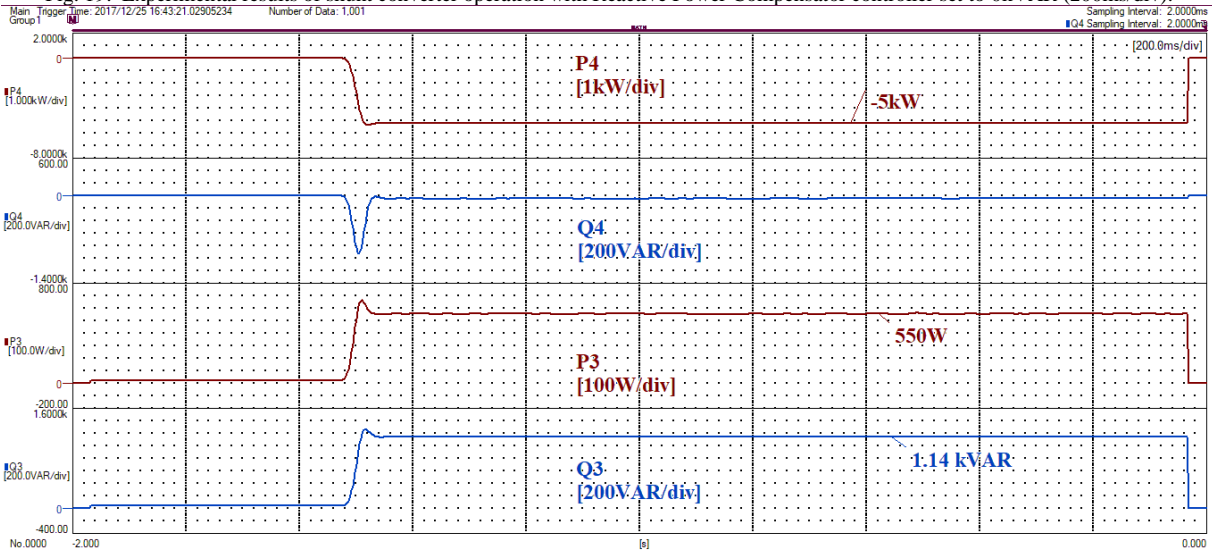550W

Q3
[200VAR/div]

1.14 kVAR

Fig. 20. Experimental results of series converter operation with Secondary Current Controller set to -5kW (200msec/div).

1kW

P1
[1 kW/div]

6.75kW

Q1
[500 VAR/div]

-230W

P2
[200 W/div]

-800W

2 kVAR

Q2
[500 VAR/div]
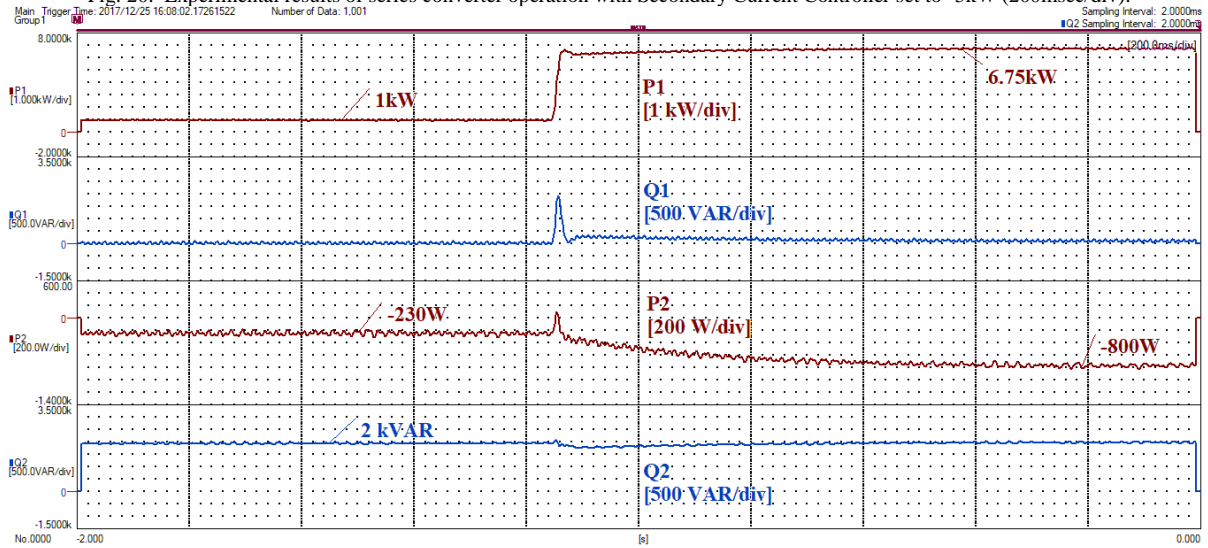
Fig. 21. Experimental results of primary and shunt winding power during activation of Secondary Current Controller set to -5kW(200ms/div).
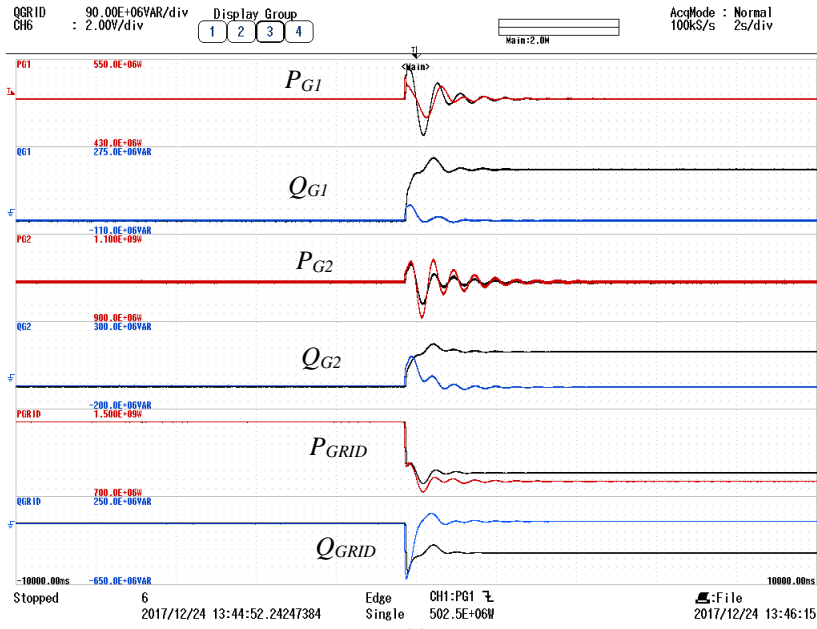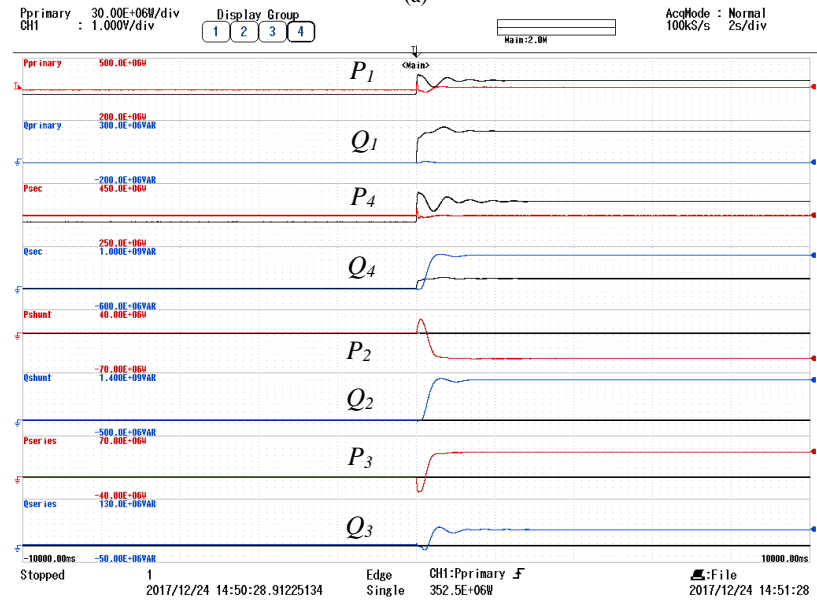
Fig. 22. Real-time simulation of the active and reactive power through the 5-bus power system with controllers disabled (black lines) and controllers enabled. (a) Grid sources and (b) CPAT windings (2sec/div).

Fig. 23. Real-time simulation of the load voltage and DC bus voltage during load connection with controllers disabled (black line) and with controllers enabled.

VI. Conclusion

This paper has presented the CPAT-UPFC consisting of three single-phase CPATs equipped with a back-to-back converter. Through the available shunt and series windings in a CPAT, several services can be supplied to the grid such as grid harmonic currents elimination, reactive power compensation and power flow control. Linear and non-linear modeling approaches of a CPAT h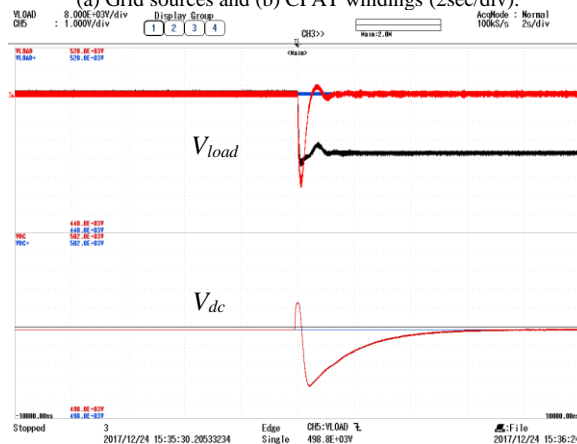as been presented and investigated under stiff-grid operation and in a 5-bus power system model. The presented control architecture has been evaluated through simulations and an experimental prototype demonstrating the ability of a CPAT to operate as a UPFC. The analysis, simulation and experimental results confirm the CPAT-UPFC ability to provide the required services.

VII. References

[1] M. S. Mahmoud, M. Saif Ur Rahman and F. M. A. L. Sunni, "Review of microgrid architectures – a system of systems perspective," IET Renewable Power Generation, vol. 9, no. 8, pp. 1064-1078, Nov. 2015.

[2] Q. Huang, S. Jing, J. Li, D. Cai, J. Wu and W. Zhen, "Smart Substation: State of the Art and Future Development," *IEEE Trans. Power Del.*, vol. 32, no. 2, pp. 1098-1105, Apr. 2017.

[3] H. Liao and J. V. Milanović, "On capability of different FACTS devices to mitigate a range of power quality phenomena," *IET Generation, Transmission & Distribution*, vol. 11, no. 5, pp. 1202-1211, Mar. 2017.

[4] M. Shahparasti, M. Mohamadian, P. T. Baboli and A. Yazdianp, "Toward Power Quality Management in Hybrid AC–DC Microgrid Using LTC-L Utility Interactive Inverter: Load Voltage–Grid Current Tradeoff," *IEEE Trans. Smart Grid*, vol. 8, no. 2, pp. 857-867, Mar. 2017.

[5] J. Barr and R. Majumder, "Integration of Distributed Generation in the Volt/VAR Management System for Active Distribution Networks," *IEEE Trans. Smart Grid*, vol. 6, no. 2, pp. 576-586, Mar. 2015.

[6] M. A. Sayed and T. Takeshita, "All Nodes Voltage Regulation and Line Loss Minimization in Loop Distribution Systems Using UPFC," *IEEE Trans. Power Electron.*, vol. 26, no. 6, pp. 1694-1703, June 2011.

[7] F. Z. Peng, "Flexible AC Transmission Systems (FACTS) and Resilient AC Distribution Systems (RACDS) in Smart Grid," *Proc. IEEE*, vol. 105, no. 11, pp. 2099-2115, Nov. 2017.

[8] E. Rakhshani, D. Remon, A. M. Cantarellas, J. M. Garcia and P. Rodriguez, "Virtual Synchronous Power Strategy for Multiple HVDC Interconnections of Multi-Area AGC Power Systems," *IEEE Trans. Power Syst.*, vol. 32, no. 3, pp. 1665-1677, May 2017.

[9] W. Litzenberger, K. Mitsch and M. Bhuiyan, "When It's Time to Upgrade: HVdc and FACTS Renovation in the Western Power System," *IEEE Power Energy Mag.*, vol. 14, no. 2, pp. 32-41, Mar. 2016.

[10] M. Andresen, K. Ma, G. De Carne, G. Buticchi, F. Blaabjerg and M. Liserre, "Thermal Stress Analysis of Medium-Voltage Converters for Smart Transformers," *IEEE Trans. Power Electron.*, vol. 32, no. 6, pp. 4753-4765, Jun. 2017.

[11] S. Yang, Y. Liu, X. Wang, D. Gunasekaran, U. Karki and F. Z. Peng, "Modulation and Control of Transformerless UPFC," *IEEE Trans. Power Electron.*, vol. 31, no. 2, pp. 1050-1063, Feb. 2016.

[12] C. Liang et al., "Harmonic Elimination Using Parallel Delta-Connected Filtering Windings for Converter Transformers in HVDC Systems," *IEEE Trans. Power Del.*, vol. 32, no. 2, pp. 933-941, Apr. 2017.

[13] C. Wang, X. Yin, Z. Zhang and M. Wen, "A Novel Compensation Technology of Static Synchronous Compensator Integrated With Distribution Transformer," *IEEE Trans. Power Del.*, vol. 28, no. 2, pp. 1032-1039, Apr. 2013.

[14] B. B. Ambati and V. Khadkikar, "Variable Frequency Transformer Configuration for Decoupled Active-Reactive Powers Transfer Control," *IEEE Trans. on Energy Convers.*, vol. 31, no. 3, pp. 906-914, Sept. 2016.

[15] J. Liu and V. Dinavahi, "Nonlinear Magnetic Equivalent Circuit-Based Real-Time Sen Transformer Electromagnetic Transient Model on FPGA for HIL Emulation," *IEEE Trans. Power Del.*, vol. 31, no. 6, pp. 2483-2493, Dec. 2016.

[16] L. Ferreira Costa, G. De Carne, G. Buticchi and M. Liserre, "The Smart Transformer: A solid-state transformer tailored to provide ancillary services to the distribution grid," *IEEE Power Electron. Mag.*, vol. 4, no. 2, pp. 56-67, June 2017.

[17] M.A. Elsaharty, J. Rocabert, I. Candela and P. Rodriguez, "Three-Phase Custom Power Active Transformer for Power Flow Control Applications," *IEEE Trans. Power Electron.*, Early Access, June 2018.

[18] M.A. Elsaharty, J.I. Candela and P. Rodriguez, "Power System Compensation Using a Power Electronics Integrated Transformer", *IEEE Trans. Power Del.*, vol. 33, no. 4, pp. 1744-1754, Aug. 2018.

[19] F. Z. Peng, Y. Liu, S. Yang, S. Zhang, D. Gunasekaran and U. Karki, "Transformer-Less Unified Power-Flow Controller Using the Cascade Multilevel Inverter," *IEEE Trans. Power Electron.*, vol. 31, no. 8, pp. 5461-5472, Aug. 2016.

[20] S. Yang, Y. Liu, X. Wang, D. Gunasekaran, U. Karki and F. Z. Peng, "Modulation and Control of Transformerless UPFC," *IEEE Trans. Power Electron.*, vol. 31, no. 2, pp. 1050-1063, Feb. 2016.

[21] Y. Liu, S. Yang, X. Wang, D. Gunasekaran, U. Karki and F. Z. Peng, "Application of Transformer-Less UPFC for Interconnecting Two Synchronous AC Grids With Large Phase Difference," *IEEE Trans. Power Electron.*, vol. 31, no. 9, pp. 6092-6103, Sept. 2016.

[22] P. Li, Y. Wang, C. Feng and J. Lin, "Application of MMC-UPFC in the 500 kV power grid of Suzhou," *The Journal of Engineering*, vol. 2017, no. 13, pp. 2514-2518, 2017.

[23] M. Andresen, K. Ma, G. De Carne, G. Buticchi, F. Blaabjerg and M. Liserre, "Thermal Stress Analysis of Medium-Voltage Converters for Smart Transformers," *IEEE Trans. Power Electron.*, vol. 32, no. 6, pp. 4753-4765, Jun. 2017.

[24] J. A. Martinez, R. Walling, B. A. Mork, J. Martin-Arnedo and D. Durbak, "Parameter determination for modeling system transients-Part III: Transformers," *IEEE Trans. Power Del.*, vol. 20, no. 3, pp. 2051-2062, July 2005.

[25] R. Teodorescu, M. Liserre, and P. Rodriguez, Grid Converters for Photovoltaic and Wind Power Systems. Hoboken, NJ, USA: Wiley, 2011.

[26] E. Rakhshani and P. Rodriguez, "Inertia Emulation in AC/DC Interconnected Power Systems Using Derivative Technique Considering Frequency Measurement Effects," *IEEE Trans. Power Syst.*, vol. 32, no. 5, pp. 3338-3351, Sept. 2017.

Mohamed Atef Elsaharty (S'12, M'13) received the B.Sc. and M.Sc. degrees in electrical and control engineering from Arab Academy for Science, Technology, & Maritime Transport (AASTMT), Alexandria, Egypt, in 2009 and 2012, respectively. He received his Ph.D. degree in Electric Energy Systems from the Technical University of Catalonia (UPC), Barcelona, Spain in 2018. Currently, he is an Assistant Professor at AASTMT since 2018. His research interests include integration of magnetic circuits and power electronics accompanied with linear and non-linear control techniques, particularly for integrated substation applications.

Alvaro Luna (S'07–M'10) received the B.Sc., M.Sc., and Ph.D. degrees from the Technical University of Catalonia (UPC), Barcelona, Spain, in 2001, 2005, and 2009, respectively, all in electrical engineering. He was a Faculty Member with the UPC in 2005, where he is currently an Assistant Professor. His research interests include wind turbines control, photovoltaic systems, integration of distributed generation, and power conditioning

Jose Ignacio Candela (S'99–M'04) received the B.S. and M.S. degrees in industrial engineering and the Ph.D. degree in electrical engineering from the Technical University of Catalonia (UPC), Barcelona, Spain, in 1987, 2000, and 2009, respectively. In 1990, he became an Assistant Professor with UPC, where he later advanced to Associate Professor in 1993 and is currently a part of the research group on Renewable Electrical Energy Systems, Department of Electrical Engineering. He has authored or co-authored more than 80 published technical papers, and holds several patents. His current research

interests include power conditioning, integration of distributed energy systems, and control of grid connected power converters.

Pedro Rodriguez (SM'10–F'13) is the Head of LOYOLA.Tech. He received the M.Sc. and Ph.D. degrees in electrical engineering from the Technical University of Catalonia (UPC), Spain. He was a postdoc researcher at the CPES, Virginia Tech, US, at the Department of Energy Technology, Aalborg University (AAU), Denmark and at the MIT Energy Initiative (MITie), Boston, US. He was a co-supervisor of the Vestas Power Program, Denmark (2007 - 2011). He was a director of technology in Modern Power Systems in Abengoa Research (2011-2017). From 2017, he is a full professor at the Loyola University Andalucia, where he is the Head of LOYOLA.Tech, leading the research programme on Intelligent Energy Systems. He is in the list of Highly Cited Researchers in Engineering (2015-2018), published by Clarivate. He has co-authored one Wiley-IEEE book, over 100 papers in ISI technical journals, and around 300 papers in conference proceedings. He is the holder of 16 licensed patents. He has participated in more than 50 projects with industrial partners and several EU projects. Dr. Rodriguez is a IEEE Fellow for his contributions in the control of distributed generation. He is an Associate Editor of the IEEE Transaction on Power Electronics and the IEEE Journal on Emerging and Selected Topics on Power Electronics. He is a member of the Sustainability and Renewable Energy Committee of the IEEE Industry Application Society and the Renewable Energy Systems Technical Committee of the IEEE Industrial Electronics Society. His research interests include intelligent energy systems, distributed generation, and rural electrification.